Eurasian Journal of Science Engineering and Technology

Research

GURSON-TVERGAARD-NEEDLEMAN (GTN) PARAMETERS OF DP STEELS WITH DIFFERENT ROLLING DIRECTIONS WERE DETERMINED AND INVESTIGATED AT DIFFERENT STRAIN RATES

Labinot TOPILLA[1,*], Serkan TOROS[2]

[1,2] *Nigde Omer Halisdemir University, Mechanical Engineering Department, 51245, Nigde, Türkiye*

ABSTRACT

Dual Phase steels are high-strength and well-formability steels, which are widely used in the automobile industry. However, based on their microstructural observations, the shapes, orientations, and directions of the grains of these two steels are different and vary depending on the degree of observation. Therefore, the objective of this research was to compare the stress and strain distribution at different strain rates of standard specimens and cut at different rolling directions of DP steels, namely DP600 and DP800 steels. Besides, in this study, the finite element modeling method is used through optimization to determine the GTN fracture failure, constitutive and nucleation parameters of the mentioned steels based on their rolling directions and strain rates. The experimental and numerical simulation results are also compared, and they are in good agreement.

Keywords: DP steels. Experimental, Optimizations, Simulations, GTN parameters.

1. INTRODUCTION

It is important to investigate high-strength and well formability steels to advance fuel efficiency, environmental protection, and vehicle safety from accidents. Strength and strain ability are characterized by a microstructure consisting of a strength martensitic phase distribution in a soft ferritic phase, which is developed in the late 1970s The term "Dual-Phase" refers to the presence of ferritic and martensitic microstructures composed of small amounts of bainite, perlite, and austenite [1]. And which are widely used in the automotive industry [2], [3] A favorable combination of strength and ductility can be obtained by developing a dual-phase or multi-phase microstructure in steel. The soft phase of steel, ferrite, has a body-centered cubic (BCC) crystal structure and can contain only a few hundredths of a percent carbon, according to [4]. The ferrite phase is the primary phase in the low range, while martensite is the generic term for microstructures formed by diffusion-free phase transformations. When the steel is annealed in the inter-critical range, it converts to austenite and ferrite, which form an FCC or BCC crystal structure. There are two basic forms of martensite structures, lath martensite, and slab martensite. While the reinforcing effect on DP structures is realized by adding martensite to the matrix ferrite. After that, the DP steels can be tensiled using conventional tools while maintaining their properties. For example, the tensile stress for DP600 steel can be increased by approximately 20% compared to micro-alloy steel (HSLA) with the same thickness. [5].

On the other hand, many finite element models determine the behavior of the material under stress-strain conditions, and so the purpose of our research was to determine the GTN parameters through finite element modeling. (MAT_GURSON_120). In addition, in 1977, Gurson proposed a yield surface based on the growth of spherical voids. This model is commonly used to describe the evolution of micromechanical damage in ductile materials. Seven years later, in 1984, Tvergaard and Needleman modified the Gurson model by introducing two additional material parameters (q1 and q2), [6]. So that the model could detect the phenomenon of cavity coalescence and the corresponding sudden loss of strength [7], since a ductile material is assumed to be porous. So, the Gurson damage model is a single-stage void model that considers the influence of void expansion on the material's plastic behaviour [8]. It is important to note that it has been recognized in recent years that the Gurson-type damage models are unable to model ductile fracture under shear dominated stress states with low-stress triaxiality [9]. There are some main parameters of the GTN damage model for a detailed analysis of the material behavior and a good understanding of the damage: the effective work-hardening parameters; the nucleation parameters; the initial porosity parameter; the yield loci parameters; and the failure parameters [10]. The modified Gurson-Tvergaard-Needleman (GTN) model is widely used in the modelling of ductile fracture [11]. As a result, this model has been adapted in many finite element programs, and it is a micromechanical damage model in which defects are assumed to exist in the materials, forming global spheres [12]. In the case of determining the GTN model parameters, the deformation curve of the stress unit, which was obtained from an experimentally used uniaxial tensile test, is required. Model parameters can be determined by adjusting the results of the finite element model, which is created by taking into account the boundary conditions of the relevant experiment. In the case of the forming process a slight deformation could be observed after the constriction, so that a break could occur even before the deformation si localized.

* Corresponding author, e-mail: labino.topilla@gmail.com (L. Topilla)
Recieved: 07.05.2022 Accepted: 18.07.2022
doi: 10.55696/ejset.1113577

Crack initiation can occur in dual-phase steel before constriction and there is a tendency for a macro crack to occur in an early state [13]. The damage curve explains the relationship between the stress triaxiality and the equivalent plastic strains [14]. Nowadays, a valuable contribution is being made by the computer field, through which it is attempted to give a continuous contribution to the knowledge of the behavior of metals during the process of deformation and failure. One of the software applications to research the behavior of materials, in general, is LS-DYNA. However, there are many models in some integrated software that mainly determine the failure and cracking of materials. The Gurson – Tvergaard – Needleman (GTN) damage model, micromechanics damage modeling (MDM), and continuum damage mechanics (CDM) are a few examples, according to [15].

Based on the literature review, no case is found where the optimization is done with finite element methods by LS-OPT, in terms of determining Gurson parameters, such as effective performance hardening parameters, nucleation parameters, initial porosity parameter, yield location parameters, and failure parameters. Therefore, by researching and considering the properties of DP600 and DP800 steels, this study aimed to contribute to the sheet metal forming industry, through describing the process of optimizations realized in LS-OPT, to determine the GTN parameters, specifically the fracture failure, the constitutive and the nucleation parameters for the mentioned steel. Morover, the aim was to determine the parameters in terms of elongation by using standard specimens resulting from different rolling directions. and tested at different strain rates, because there appear to be changes in strain, see Tables 3 and 5. Because the microstructure of Dual Phases steel is known to be mostly composed of the ferrite phase, which offers ductility, and the martensite phase, which provides strength. However, the shapes, orientations, and directions of the grains of these two phases are different and vary depending on the degree of observation. Finally, based on our research done in the literature, so far we have not found any research similarities with our research goals.

2. MATERIAL AND METHOD

2.1 Experimental procedure

In the following Figures 1, and 2, are presented the comparisons between experimental results of DP600, and DP800 steels, cut at 0°, 45°, and 90° degrees of rolling directions (RD). The specimens were based on the ASTM E8 standard, and with average properties equipped with a 50 mm gauge length, a nominal thickness of 0.78 mm, and a width of 12.5 mm. Where the preformation of the experimental, uniaxial tensile test was done at room temperature and at strain rates 0.0083 s^{-1}, 0.042 s^{-1}, and 0.16 s^{-1}. In the mentioned figures, the graphical representation of mechanical properties is presented. And the curves are realized based on the general engineering stress-strain equation. Figure 1 shows graphical comparisons of engineering stress-strain curves of DP600 steel cut at 0°, 45°, and 90° degrees (RD) and tested at three different strain rates. While In Figure 2. (a, b, and c) are the graphical comparison representations of engineering stress-strain curves of DP800 steel, cut at 0°, 45°, and 90° degrees (RD), and tested at three different strain rates too. While their differences are expressed in tabular form in terms of elongations, they are presented in Tables 3 and 5.

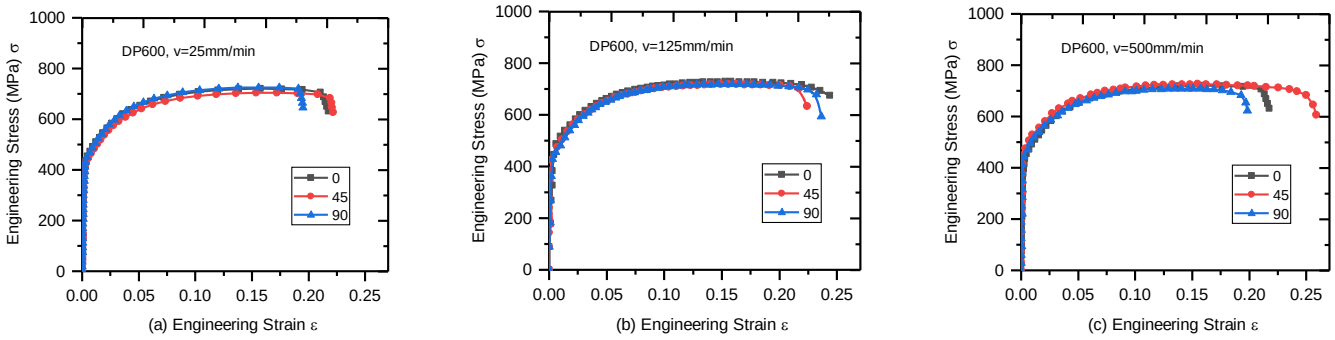

Figure 1 Comparison of force displacement results of DP600 steel as a result of different rolling directions and different strain rate

GURSON-TVERGAARD-NEEDLEMAN (GTN) PARAMETERS OF DP STEELS WITH DIFFERENT ROLLING DIRECTIONS WERE DETERMINED AND INVESTIGATED AT DIFFERENT STRAIN RATES

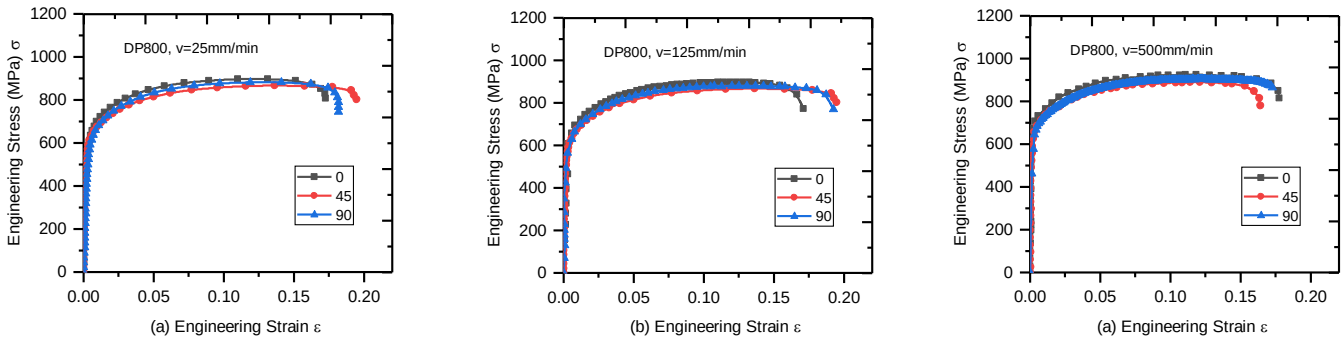

Figure 2. Comparison of force displacement results of DP800 steel as a result of different rolling directions and different strain rate

The microstructure of DP600 and DP800 steels based on microscopic observation is shown in Figures 3 and 4. The aim was to give a visual view of the orientation of the grains seen from a different angle of rolling direction (RD). Figures 3. (a) and 4. (a) show the view of the microstructure when viewed from an angle of 0° of RD, whereas Figures 3. (b) and 4. (b) shows the view of the microstructure when viewed from an angle of 45° of RD. In figures 3. (c) and 4. (c), microstructure images are presented when viewed from an angle of 90° of RD. The martensite phase is shown in black, while the ferrite phase is shown in yellow.

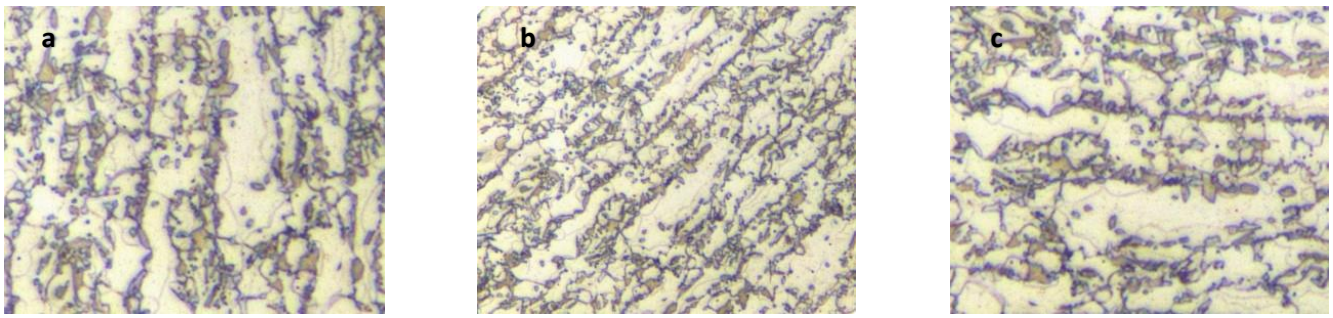

Figure 3. Microstructure observation of DP600 steel from different rolling directions

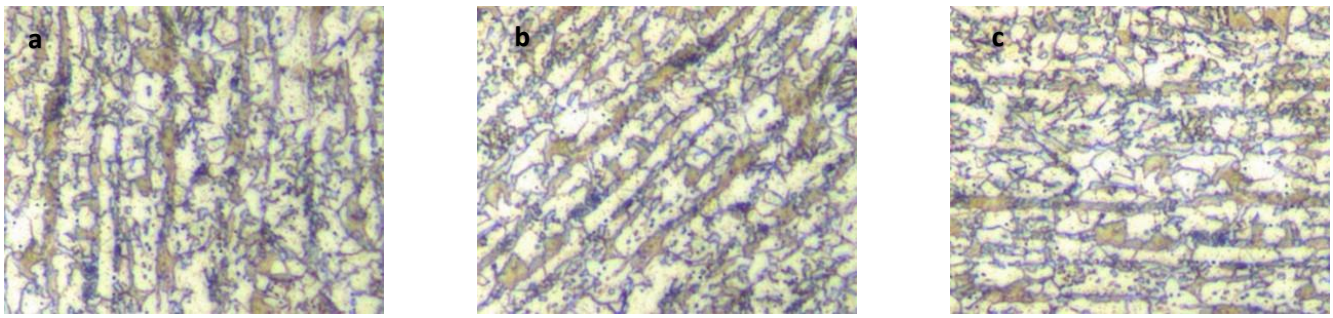

Figure 4. Microstructure observation of DP800 steel from different rolling directions.

2.2 Numerical modeling of ductile damage Gurson_120_Mat_Model

This model, which has been adapted into most finite element software, is basically a micromechanical damage model that assumes that defects are already present in materials and that these defects form spherical voids. Standard uniaxial tensile testing, microstructural characterization, and finite element modeling were used to assess the continuity of damage behavior investigations in the DP600 and DP800 steels investigated by [18] on the void analysis and experimental data of the uniaxial

traction test, and the determination of the damage parameters of the Gurson-Tvergaard-Needleman (GTN) damage model. As a result, a good agreement is reached between the predictions and the experimental load elongation, allowing the identification of the complete set of parameters of the GTN damage model of the DP600 and DP800 steels. According to [16] which emphasize that physical approach that introduces a damage model coupled with the behavior of porous materials was the Gurson theory.

$$\Phi = \left(\frac{q}{\sigma_0}\right)^2 + 2f\cosh\left(-\frac{3p}{2\sigma_0}\right) - 1 - f^2 = 0 \quad (1)$$

where σ_0 is the flow stress of the material, f represents the voids volume fraction of the material, $q = \sqrt{(3/2)}\, s{:}s$ is the von Mises equivalent stress with s is the deviatoric part of the stress tensor and $p = -trace(\sigma)/3$ is the hydrostatic stress. The original Gurson model was later modified by Tvergaard and Needleman and started to be referred to as the GTN criterion. During the determination of the GTN model parameters, the stress strain curve obtained from an experimentally applied tensile test is needed. The model parameters can be determined by adapting the results obtained from the finite element model created by considering the boundary conditions of the relevant experiment to the experimental results. The formulations related to the GTN model are given below. The Gurson flow function is defined as:

$$\Phi = \frac{\sigma_M^2}{\sigma_y^2} + 2q_1 f^* \cosh\left(\frac{3q_2\sigma_H}{2\sigma_y}\right) - 1 - (q_1 f^*)^2 = 0 \quad (2)$$

The *q1* and *q2* parameters in Equation 3 were added to the model by Tvergaard and are two important parameters for improving the model prediction performance. With the expression *f* in the model, it shows the amount of defects in the material and is determined as follows.

$$f^*(f) = \begin{cases} f & f \le f_c \\ f_c + \frac{1/q_1 - f_c}{f_F - f_c}(f - f_c) & f > f_c \end{cases} \quad (3)$$

While the defect rate is taken until the defects that occur with the deformation in the material reach a certain level, the calculations in the 2nd step are made if it exceeds the critical value. However, according to the studies of Gurson Tvergaard and Needieman, and Nahshon and Hutchiston, the increase in voids in the material internal structure can be expressed by Equation 4-7. The growth of the void volume fraction is defined as

$$\dot{f} = \dot{f_G} + \dot{f_N} \quad (4)$$

where the growth of existing voids is defined as

$$\dot{f_G} = (1 + f)\ \dot{\varepsilon}_{kk}^p \quad (5)$$

and the nucleation of new voids is defined as

$$\dot{f_N} = A\dot{\varepsilon}_p, \quad \text{Where} \quad (6)$$

$$A = \frac{f_N}{S_N\sqrt{2\pi}} exp\left(-\frac{1}{2}\left(\frac{\varepsilon_p - \varepsilon_N}{S_N}\right)^2\right) \quad (7)$$

The *fo, fN, fc and ff* values in the given models should be determined and introduced to the programs.

2.3 Finite Element Modeling For Gurson Model

The solid element was used for MAT_GURSON_120 MODEL during the construction of kye cards to perform numerical optimizations and simulations. It is understood that all the properties of the mechanical data placed on the key cards are similar to the experimental data, including similarity to geometric shapes of specimens, size, thickness, width, time duration, and even strain rate, applied to perform uniaxial tensile testing. Along with the GTN parameters: ε_N, f_c, f_f, f_N ,q_1 ,q_2, S_N, mechanical properties such as density (p = 7.830e-06), Young module (E = 216), and Poisson ratio (v = 0.28) are included in the key cards. While at load curve ID: LCSS =, each specimen was given its own experimental Hollomon's curve. Nevertheless, regarding this model, [10] have contributed to explaining the GTN parameters. Figure 5. will show the mash and the geometric shapes of the used specimens.

Figure 5. The finite element mesh of the ASTEM E8 uniaxial tensile test specimen

2.4 Theory of optimization

Optimization can be defined as a procedure for "achieving the best outcome of a given operation while satisfying certain restrictions." This objective has always been central to the design process but is now assuming greater significance than ever because of the maturity of the mathematical and computational tools available for design. Solving the optimization problem requires an optimization algorithm. The two basic optimization branches employed in LS-OPT are metamodel-based optimization and direct optimization [17]. The optimizations of Gurson parameters were realized in the application software LS-OPT (metamodel-based optimization). For the mentioned model, a total of 18 specimens were optimized separately, one by one, followed by a 10 x 10 itineration. In the LS-OPT software are placed all the necessary mechanical and geometric dates, which are similar to the experimental results and key cards. While, in the setup, the parameters for the optimizations expressed at the starting, minimum, and maximum are set. See tables 1–2. As all investigated cases result in different parameters as mentioned [6] the choice of different tests could result in different parameter values for the modified Gurson model. See the optimization process in Figure 6.

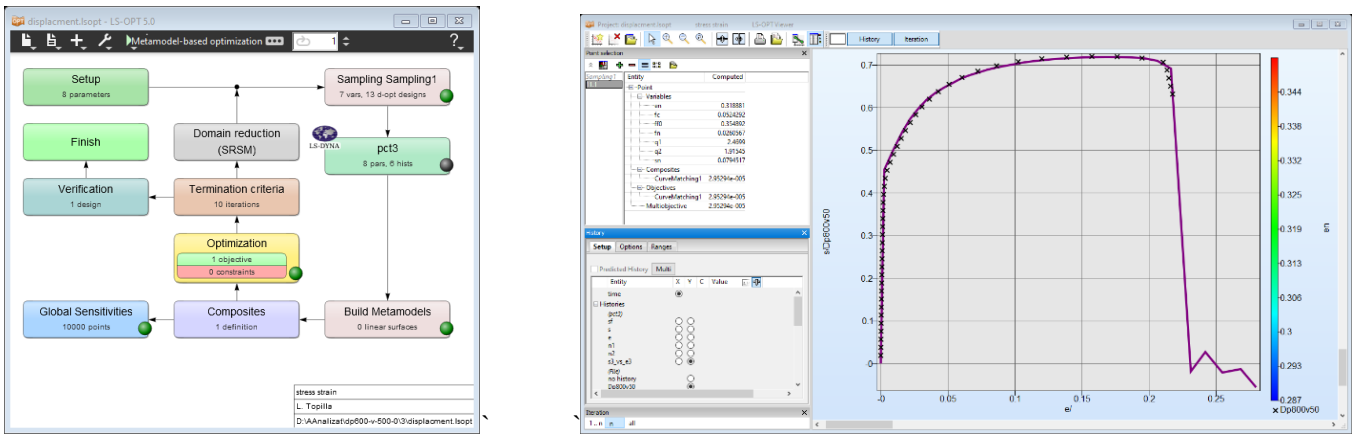

Figure 6. LS-OPT optimization figurative process in Figure 6

3 RESULTS AND DISCUSSION

3.1 Results and Discussion of GTN parameters

Parameters ε_N, $and\ S_N$ usually have their standard values from 0.1 up to 0.3, and mostly for DP steels. Therefore, these are thought of as statistical constants of nucleation and not as internal proportions of materials [11]. So, S_N, is the standard deviation, f_N is the volume fraction of particles, and during the material deformation process, the f_N stands for volume fraction when voids nucleate. And the meaning of ε_N, value is the strain when void nucleation happens. The influence of value ε_N, is interrelated with the influence of [11]. While in our case, the aforementioned materials are used as working parameters ε_N, S_N, $and\ f_N$ during the optimization process, the starting parameters for DP800 steels were defined as $\varepsilon_N, = 0.065 - 0.085$: and the maximum variates ranged from: 0.27-32. It is important to note that this was a key parameter that had a large impact on defining the curve fitting. While S_N the starting parameters were set to be: 0.05–0.1, the maximum was set to: $S_N = 0.25 - 0.3$. The following are the starting parameters: $f_N = 0.01$ and the maximum is given by: $f_N = 0.05$. Where's for DP600 steels, for parameter ε_N starting were defined to be: $\varepsilon_N, = 0.06 - 0.09$ and the maximum variations range from 0.27 to 35. In terms of S_N parameters, the minimum was set to 0.03 and the maximum was set to: $S_N = 0.25 - 0.3$. For f_N parameter the starting point was defined as: $f_N = 0.0104$ and the maximum as: $f_N = 0.05$. Tables 1–2 show the results.

Table 1. Exhibit optimisation parameters prediction of GTN of DP600 steels.

Specimens	Parameter	ε_N	f_c	f_f	f_N	q_1	q_2	S_N
DP600, 0° 0.00833 s^{-1}	Starting	0.06	0.016	0.22	0.0104	1.84	0.8	0.28
	Minimum	0.01	0.002	0.001	0.003	0.45	0.3	0.03
	Maximum	0.30	0.052	0.62	0.05	2.5	2.21	0.25
	Results	0.2816	0.002	0.3704	0.0171	2.1981	1.9287	0.0438
DP600, 0° 0.042 s^{-1}	Starting	0.09	0.013	0.25	0.0104	1.86	0.8	0.03
	Minimum	0.01	0.002	0.001	0.003	0.45	0.3	0.013
	Maximum	0.34	0.53	0.61	0.05	2.5	2.2	0.25
	Results	0.0138	0.3955	0.5505	0.0199	1.9922	1.3056	0.2019
DP600, 0° 0.16 s^{-1}	Starting	0.09	0.012	0.21	0.0104	1.86	0.8	0.03
	Minimum	0.01	0.002	0.001	0.003	0.45	0.3	0.013
	Maximum	0.35	0.50	0.63	0.05	2.5	2.2	0.25
	Results	0.3188	0.0524	0.3540	0.0260	2.4699	1.9154	0.0794

Table 2. Exhibit optimisation parameters prediction of GTN of DP800 steel.

Specimens	Parameter	ε_N	f_c	f_f	f_N	q_1	q_2	S_N
DP800, 90° 0.00833 s^{-1}	Starting	0.065	0.0091	0.17	0.01	1.7	0.8	0.1
	Minimum	0.05	0.001	0.003	0.003	0.45	0.3	0.033
	Maximum	0.27	0.7	0.8	0.05	2.5	1.8	0.25
	Results	0.2614	0.0020	0.3274	0.0430	1.0966	1.0715	0.0660
DP800, 45° 0.042 s^{-1}	Starting	0.085	0.0057	0.16	0.01	1.5	0.8	0.1
	Minimum	0.05	0.002	0.001	0.003	0.45	0.3	0.033
	Maximum	0.28	0.65	0.84	0.05	2.5	1.8	0.25
	Results	0.2230	0.1722	0.1926	0.0324	1.6605	1.5819	0.0653
DP800, 0° 0.16 s^{-1}	Starting	0.085	0.0058	0.17	0.01	1.7	0.8	0.05
	Minimum	0.01	0.002	0.001	0.003	0.45	0.3	0.033
	Maximum	0.28	0.73	0.7	0.05	2.5	1.8	0.25
	Results	0.2636	0.4370	0.4572	0.0206	2.2835	1.8	0.033

3.3 Constitutive parameters

The constitutive parameters introduced by Tvergaard and Needleman (q_1- q_3) [18] or the yield locus parameters [10], usually thought to be fixed: $q_1 = 1.5$, $q_2 = 2$, $q_3 = q_1^2$ [19]. However, by optimizing DP00 and DP800 steels with their tested properties, These q_1 and q_2 parameters are being used in each case, So, for DP800 steel, the starting point was set to q_1 = 1.7 and the maximum was set to q_1 =2.5. As for q_2 the starting point was set to be $q_2 = 0.8$, and the maximum range was set to 1.8-2.2. While, for DP600 steel q_1 starting were defined to be: $q_1 = 1.86$ and the maximum were given by: 2.5, as for q_2 starting were defined to be: $q_2 = 0.8$ and the maximum were given to be: 2.2.

3.4 Failure Parameters

The porosities, f_c and f_f are considered material parameters and there are several methods to determine them, especially the critical void volume fraction, which is the failure parameter f_c, and corresponds to the onset of void coalescence. Also f_c can be numerically obtained by fitting the numerical curve with the experimental one [11]. But in the respective study, the determination of the critical void volume fraction f_c is obtained from the plastic strain corresponding to the ultimate yield strength[10], Because when the deformation reaches this point, then it starts to take the form of plastic deformation as the pores begin to settle and the whole coalescence is created. While the failure parameter (the final void volume fraction) f_f is obtained from the plastic deformation at the moment of falling, at the cross-sectional area, when the curve downwards or when the stress loses its carrying ability completely. In this diagram Figure 7 are presented the targeting of f_c and f_f parameters for optimization

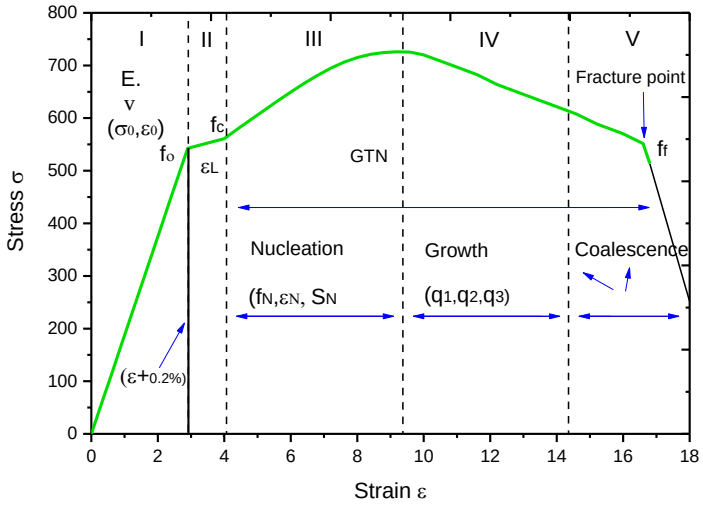

Figure 7. The graphic explanation of defining the GTN model parameters can be subdivided into three subsets.

3.5 Comparison between the model predictions and experimental results of DP600 steel, ε_r = 0.0083 s^{-1}, at different rolling directions (RD)

The comparison of the experimental and numerical simulation results obtained from the d3plot file generated after the optimizations are shown in the following figures. The compared properties are listed above in Table 3, while the GTN parameters are shown in Table 4. Figures 8, 9. and 10 show the comparisons between experimental and numerical curves and the mechanical properties of standard specimens of DP600 steel cut at 0°, 45° and 90° to the rolling direction (RD). The experimental and numerically simulated uniaxial tensile tests were performed at a strain rate of ε_r = 0.0083 s^{-1} for all specimens studied. These curve comparisons agree well with the results of [14] for all tests in terms of fracture displacement. As a result, the graphical comparisons of mechanical properties are based on the general stress-strain equation and are shown in Figures 8, 9, and 10. (a) depicts the graphical comparisons of engineering stress-strain curves. Figures 8, 9. and 10, (b) show the graphical comparisons of the true stress-strain curves, and Figures 8, 9. and 10, (c) show the graphical comparisons of the Hollomon plastic deformation flow curve.

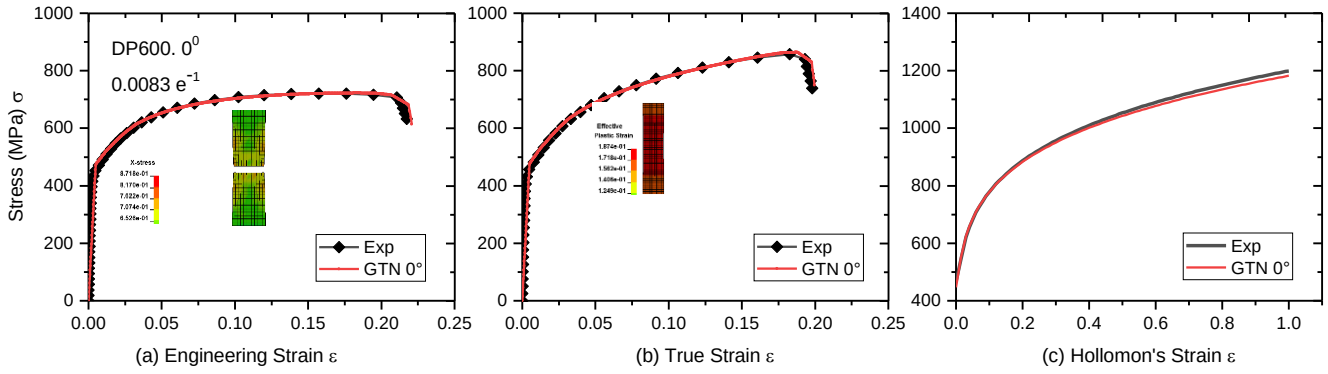

Figure 8. Compariosns between experimental and numerical simulation results of DP600 steel, RD = 0°, ε_r = 0.0083 s^{-1}, (a) σ_{eng}, (b) σ_{true}, (c) Hollomon curve

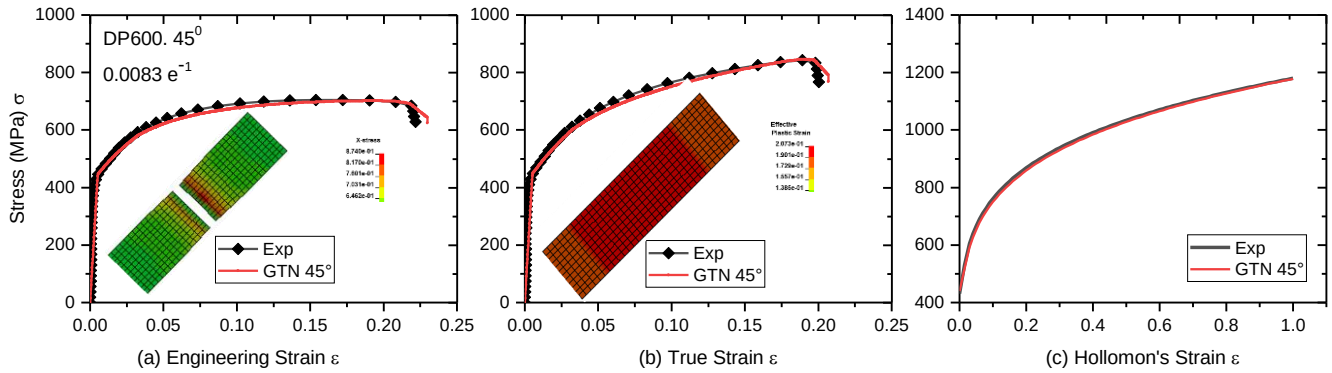

Figure 9. Compariosns between experimental and numerical simulation results of DP600 steel, RD = 45°, $\boldsymbol{\varepsilon_r}$ = 0.0083 s^{-1}, (a) $\boldsymbol{\sigma_{eng}}$, (b) $\boldsymbol{\sigma_{true}}$, (c) Hollomon curve

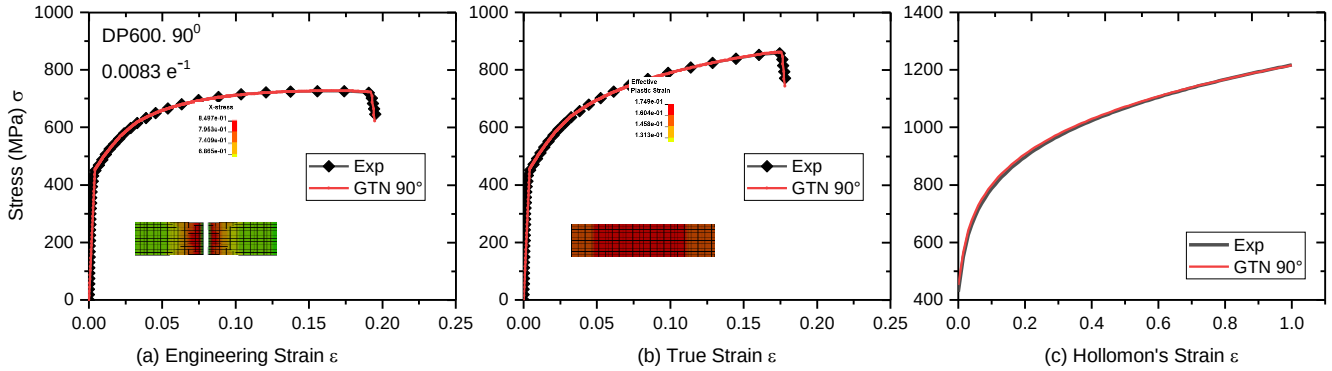

Figure 10. Compariosns between experimental and numerical simulation results of DP600 steel, RD = 90°, $\boldsymbol{\varepsilon_r}$ = 0.0083 s^{-1}, (a) $\boldsymbol{\sigma_{eng}}$, (b) $\boldsymbol{\sigma_{true}}$, (c) Hollomon curve

In this section, relative errors (RE) between experimental results and numerical simulation results for DP600 steel with different rolling directions (RD) and tested at a strain rate $(\varepsilon_r)\ of,\ \varepsilon_r$ = 0.0083 s^{-1}, a are presented. Comparisons were made for all specimens tested, with particular emphasis on engineering fracture strain. (ε_{eng_f}), true fractures strain (ε_{true_f}), and Hollomon ultimate tensile strength (σ_H), Hence, in Figure 8, are presented relative errors (RE) calculations of DP600 steel, RD = 0°. And from the numerical calculation of the RE that was done for the engineering fracture strain (ε_{eng_f}) this is the result of RE = 1.05%, whereas, for the true fractures strain (ε_{true_f}) this is the result of RE = 1.01%, and regarding Hollomon flow curve (σ_H) this is the result of RE = 1.44%. Whereas, Figure 9 presents RE calculations for the same steel, but with a different RD = 45°. And from the mathematical calculation of the difference that has been done for the engineering fracture strain (ε_{eng_f}) this is the result of RE = 3.10%, while, for the true fractures strain (ε_{true_f}) this is the result of RE = 2.9%, and for Hollomon flow curve (σ_H) this is the result of RE = 1.17%. Finally, Figure 10. presents RE calculations for the mentioned steel, also with a different RD = 90°. And from the mathematical calculations of the RE that were done for the engineering fracture strain (ε_{eng_f}) this is the result of RE = 0.05%, while for the true fractures strain (ε_{true_f}) this is the result of RE = 0.00%, and for Hollomon flow curve (σ_H) this is the result RE = 0.16%.

The mechanical properties of DP600 steel obtained from the experimental and numerical simulation results of true-stress-strain measures of specimens tested at three different rolling directions and three different strain rates are summarized in Table 3. These properties include true ultimate tensile strength (σ_u), Holloman's ultimate tensile strength(σ_H), and true fracture strain (ε_{true_f}) comparisons are similar [10]. While Figure 11 represents graphically the comparisons for true fracture strain.

Table 3. Comparisons between experimental and numerical simulation results of the mechanical properties of DP600 steel.

DP600		(σ_u) (Mpa)		Hollomon (σ_H) Mpa		Fracture (ε_{true_f})	
Specimens	Velocity	Exp	Sim	Exp	Sim	Exp	SIM
S - RD=0°	0.00833 s^{-1}	858	863	1199	1182	0.197	0.199
S - RD=45°		842	846	1179	1177	0.201	0.207
S - RD=90°		857	862	1217	1215	0.178	0.178
S - RD=0°	0.042 s^{-1}	873	866	1192	1173	0.22	0.221
S - RD=45°		859	855	1190	1159	0.2	0.211
S - RD=90°		858	867	1206	1193	0.21	0.213
S - RD=0°	0.16 s^{-1}	856	857	1164	1181	0.196	0.197
S - RD=45°		872	865	1149	1139	0.23	0.235
S - RD=90°		826	834	1155	1139	0.18	0.182

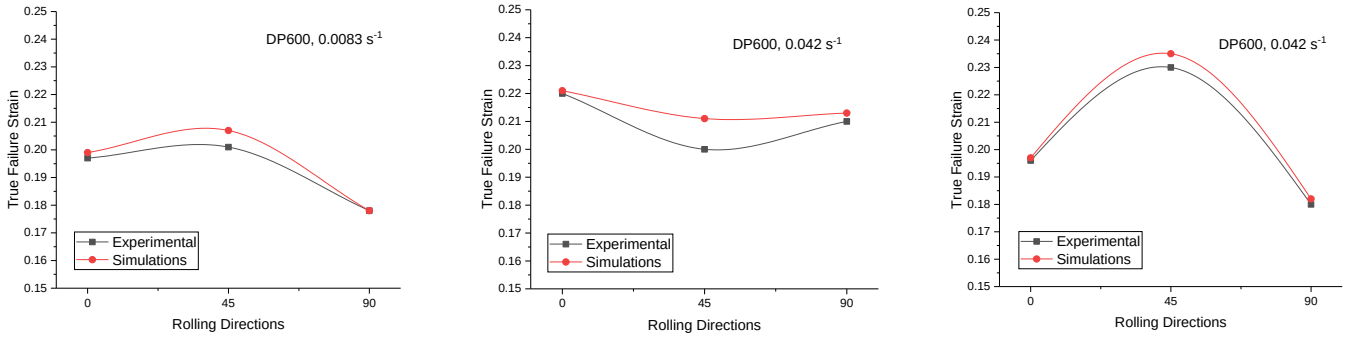

Figure 11. Experimental and simulation comparisons of DP600 steel as a result of different rolling directions and different strain rate.

The GTN parameters that are presented in table 4 are obtained from the optimization with special emphasis on the samples mentioned. All these final results have been leaked as a result of the optimization made in LS-OPT, separately for each specimen.

Table 4. Exhibit parameters prediction of GTN of DP600 steel.

Specimens	**GTN Parameters**	ε_N	f_c	f_f	f_N	q_1	q_2	S_N
DP600, 0°,	**0.00833 s^{-1}**	0.2816	0.002	0.3704	0.0171	2.1981	1.9287	0.0438
DP600, 45°,	**0.00833 s^{-1}**	0.2596	0.0037	0.1601	0.0119	2.2461	1.7898	0.0485
DP600, 90°,	**0.00833 s^{-1}**	0.1032	0.4010	0.0211	0.0212	1.8589	1.6026	0.1687
DP600, 0°,	**0.042 s^{-1}**	0.0138	0.3955	0.5505	0.0199	1.9922	1.3056	0.2019
DP600, 45°,	**0.042 s^{-1}**	0.2633	0.2917	0.1881	0.0224	1.9635	1.808	0.0212
DP600, 90°,	**0.042 s^{-1}**	0.29	0.2152	0.4143	0.0038	2.2369	2.2	0.0978
DP600, 0°,	**0.16 s^{-1}**	0.3188	0.0524	0.3540	0.0260	2.4699	1.9154	0.0794
DP600, 45°,	**0.16 s^{-1}**	0.35	0.1344	0.4597	0.0103	1.1613	1.9352	0.0158
DP600, 90°,	**0.16 s^{-1}**	0.1909	0.1062	0.4245	0.0135	2.3191	1.9536	0.0174

3.6 Comparison between the model predictions and experimental results of DP800 steel, ε_r= 0.0083 s^{-1}, at different rolling directions (RD)

In addition to the results obtained from the d3plot file simulation as a result of the optimization, the comparisons between the experimental results and the numerical simulation results are presented graphically. In terms of steel DP800, cut at RD 0°, 45°, and 90°, performing the uniaxial tensile test for both analyses with a strain rate of ε_r= 0.0083 s^{-1}. Those curve comparisons are in good agreement for all tests in terms of fracture displacement, with a difference of less than 1.5%, as shown in [6]. In

Table 5, the comparisons that belong to the mechanical properties are listed. Also in Table 6, the GTN parameters are listed for all the comparison specimens. In the following Figures 12.13, and 14, the comparisons between experimental and numerical simulation are shown graphically: Figures 12, 13 and 14 (a) show the graphical comparisons of the engineering stress-strain curves; Figures 12. 13 and 14. (b) show the graphical comparisons of the true stress-strain curves; and Figures 12. 13 and 14. (c) shows the graphical comparisons of Hollomon plastic deformation.

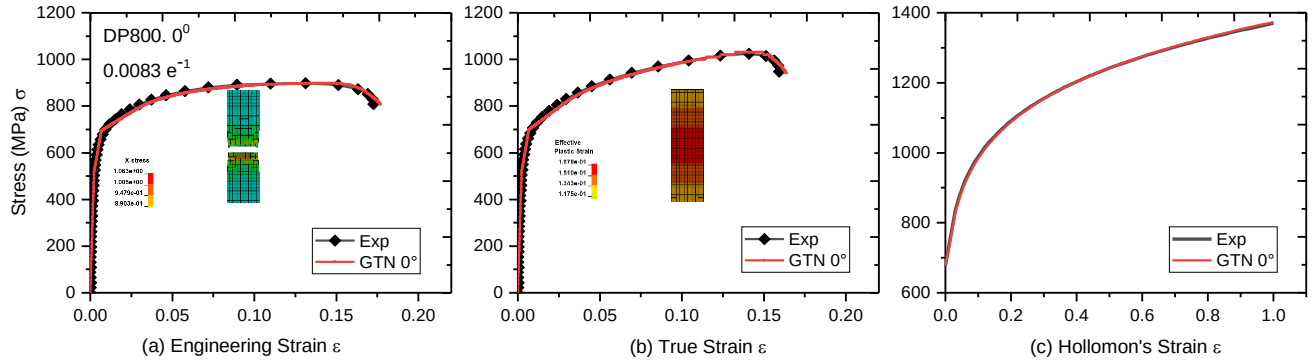

Figure 12. Compariosns between experimental and numerical simulation results of DP800 steel, RD = 0°, $\boldsymbol{\varepsilon_r}$= 0.0083 s^{-1}, (a) $\boldsymbol{\sigma_{eng}}$, (b) $\boldsymbol{\sigma_{true}}$, (c) Hollomon curve Ɛ

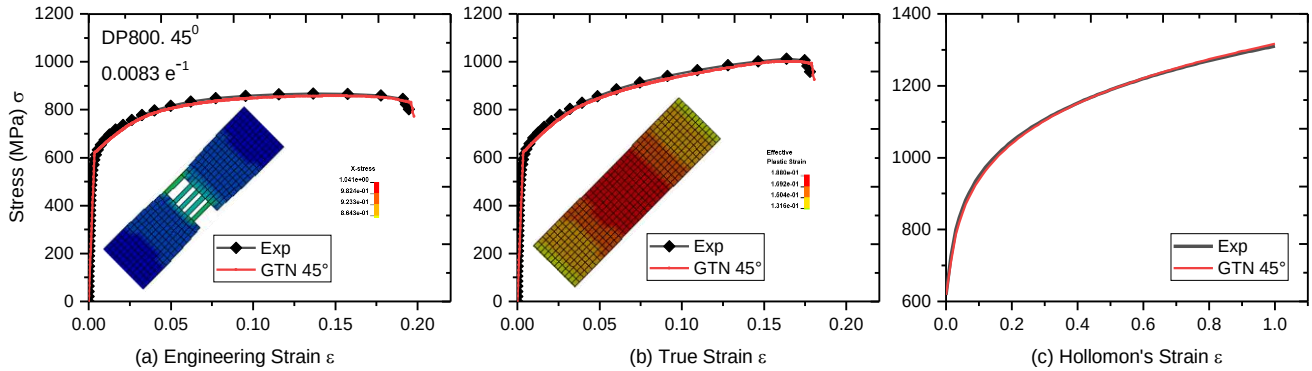

Figure 13. Compariosns between experimental and numerical simulation results of DP800 steel, RD = 45°, ε_r= 0.0083 s^{-1}, (a) σ_{eng}, (b) σ_{true}, (c) Hollomon curve

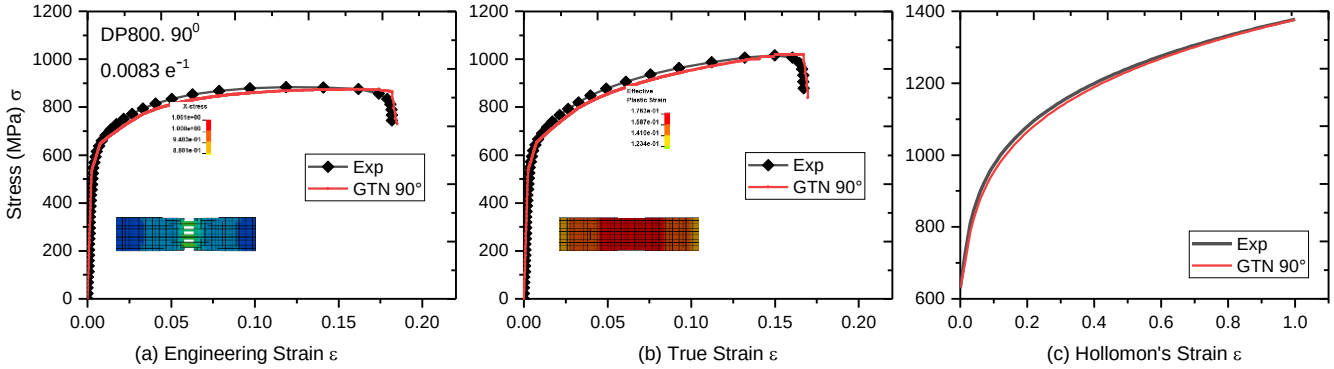

Figure 14. Compariosns between experimental and numerical simulation results of DP800 steel, RD = 90°, ε_r= 0.0083 s^{-11}, (a) σ_{eng}, (b) σ_{true}, (c) Hollomon curve

GURSON-TVERGAARD-NEEDLEMAN (GTN) PARAMETERS OF DP STEELS WITH DIFFERENT ROLLING DIRECTIONS WERE DETERMINED AND INVESTIGATED AT DIFFERENT STRAIN RATES

In this part, relative errors between experimental results and numerical results are for DP800 steel specimens with different rolling directions, tested at a strain rate (ε_r) of ε_r= 0.0083 s^{-1}. As well, comparisons were made for all specimens tested with particular emphasis of engineering fractures strain (ε_{eng_f}), true fractures strain (ε_{true_f}), and Hollomon ultimate tensile strength (σ_H). Similarly, Figure 12. represents relative errors in calculations of the mentioned steel, RD = 0°. Hence, the relative errors defined for engineering fracture strain is (ε_{eng_f}) is RE = 2.49%, for true fractures strain (ε_{true_f}) is RE = 2.45%, and for Hollomon flowe curve (σ_H) is RE = 0.29%. Figure 13 shows relative error calculations for the previously mentioned steels, but with varying RD = 45°. Where the relative errors defined regarding engineering fracture strain (ε_{eng_f}) is RE = 1.74%, true fracture strain (ε_{true_f}) is RE = 1.67%, and for Hollomon flowe curve (σ_H) is RE = 0.46%. Finally, Figure 14 shows relative error calculations for the same steel with a different RD = 90°. As a result, the engineering fracture strain defines the relative errors. (ε_{eng_f}) results is RE = 1.33%, and from true fractures strain (ε_{true_f}) results is RE = 1.18%, while from Hollomon flowe curve (σ_H) results RE = 0.15%.

Table 5 summarizes the mechanical parameters of DP800 steel derived from experimental and numerical simulations of true-stress-strain measures of specimens evaluated in three distinct rolling directions and three different strain rates. These properties include true ultimate tensile strength (σ_u), Holloman's ultimate tensile strength(σ_H), and true fracture strain (ε_{true_f}) comparisons are similar [10]. Figure 15 shows the comparisons for true fracture strain graphically.

Table 5. Comparisons between experimental and numerical simulation results of the mechanical properties of DP800 steel.

DP800		**(σ_u) (Mpa)**		**Hollomon (σ_H) (Mpa)**		**Fracture (ε_{true_f})**	
Specimens	Velocity	Exp	Sim	Exp	Sim	Exp	SIM
S - RD=0°	0.00833 s^{-1}	1024	1030	1369	1373	0.159	0.163
S - RD=45°		1012	1000	1310	1316	0.177	0.180
S - RD=90°		1016	1020	1378	1376	0.167	0.169
S - RD=0°	0.042 s^{-1}	1020	1030	1328	1400	0.159	0.162
S - RD=45°		1012	996	1310	1319	0.177	0.178
S - RD=90°		1021	1030	1348	1358	0.176	0.178
S - RD=0°	0.16 s^{-1}	1053	1060	1328	1384	0.163	0.165
S - RD=45°		1009	1010	1288	1321	0.152	0.154
S - RD=90°		1070	1072	1368	1370	0.18	0.182

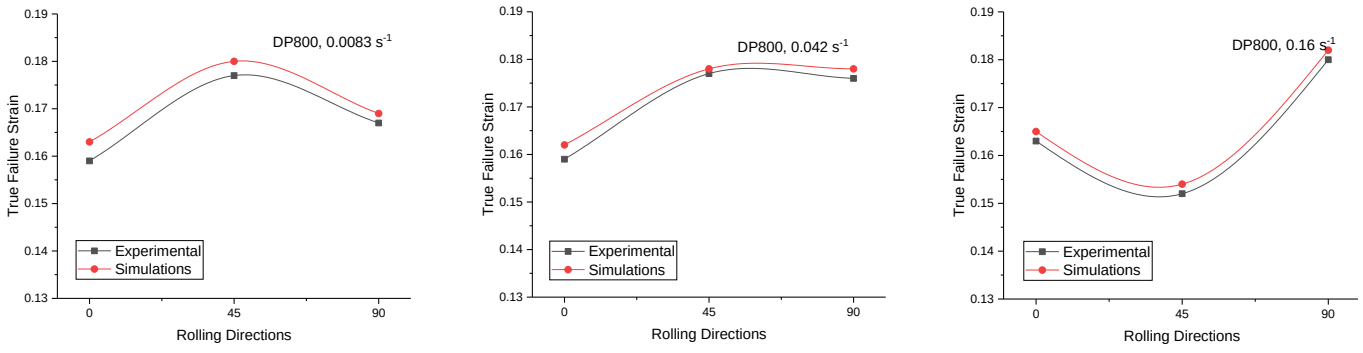

Figure 15. Experimental and simulation comparisons of DP800 steel as a result of different rolling directions and different strain rate.

The GTN parameters obtained from the optimization are presented in Table 6, with special emphasis on the samples mentioned in the table. All these final results were leaked as a result of the optimization made in LS-OPT, separately for each specimen.

Table 6. Exhibit parameters prediction of GTN of DP800 steel. ε_r= 0.0083 s^{-1}

Specimens GTN Parameters	ε_N	f_c	f_f	f_N	q_1	q_2	S_N
DP600, 0°, 0.00833 s^{-1}	0.2614	0.0020	0.3274	0.0430	1.0966	1.0715	0.0660
DP600, 45°, 0.00833 s^{-1}	0.3199	0.2196	0.7314	0.0144	0.8610	2.2	0.0378
DP600, 90°, 0.00833 s^{-1}	0.2693	0.4604	0.6357	0.0756	1.7334	1.8272	0.0345
DP600, 0°, 0.042 s^{-1}	0.2230	0.1722	0.1926	0.0324	1.6605	1.5819	0.0653
DP600, 45°, 0.042 s^{-1}	0.3199	0.2196	0.7314	0.0144	0.8610	2.2	0.0379
DP600, 90°, 0.042 s^{-1}	0.2620	0.1862	0.6617	0.0206	1.9337	1.8	0.0447
DP600, 0°, 0.16 s^{-1}	0.2636	0.4370	0.4572	0.0206	2.2835	1.8	0.033
DP600, 45°, 0.16 s^{-1}	0.2084	0.5074	0.3838	0.0192	2.5	1.8	0.0392
DP600, 90°, 0.16 s^{-1}	0.2493	0.0039	0.475	0.0351	1.0737	1.7999	0.0477

In relation to the numerical simulation results of the GTN model, and comparisons between specimens regarding effective plastic strain are particularly important, because their FEM values are similar to experimental values. Moreover, Figure 16. (a) depicts comparisons of EPS regarding DP600 steel, while Figure 16. (b) shows the comparison between numerical simulation results in the area of ESP regarding DP800 steel. These results are obtained from the simulations, which can be seen in Figures (b) from 8–14. Also, X stress in parallel with EPS was obtained.

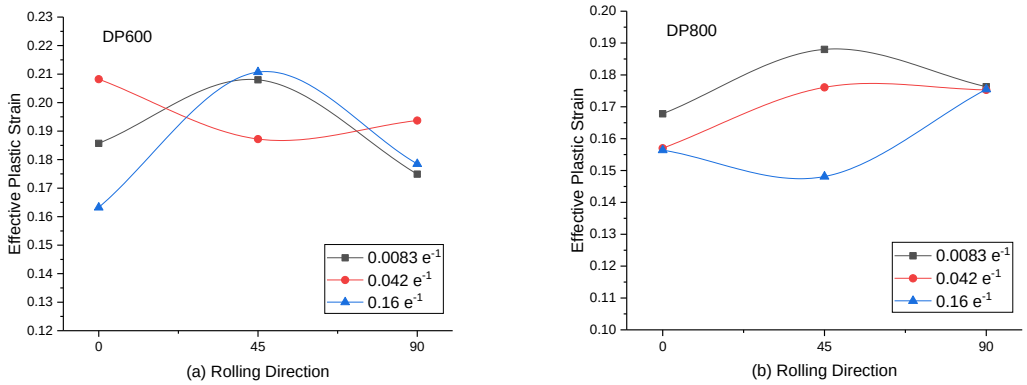

Figure 16. Finite element modeling comparisons of effective plastic strain between specimens tested at different strain rates with different rolling directions, (a) DP600 steel (b), DP800 steel

4. CONCLUSION

The presented work is divided into two parts of the study: the experimental study and the finite element modeling study.

The purpose of the experimental study was to investigate the behavior of steels cut from three different rolling directions and tested at three different strain rates. And as a result of this research, it turns out that the samples that belong to the same material but when their cutting was done in different angles, when thay were tested, they present different strain from each other, and all these changes stem from the orientations of the grains in the microstructure. Also, for the same samples, when analyzing is done at different strain rate, they show different extensions too. All experimental results were compared with each other by comparing the tested samples, which had similar strain rates but that the angle of prairie or rolling directions was different, and their results are given in the above figures.

On the other hand, in terms of finite element modeling, the aim was to find all GTN parameters through the optimization method that was realized in LS-OPT. Also, all the necessary parameters for the realization of optimizations are defined. The values of effective plastic strain that appear as a result of the finite element modeling results, as well as modeling stress displayed as x-stress, when they are compared with the experimental results, they have very good similarities. This means that the degree of strain and stress can be determined by paying attention to these FEM values. Finally, this optimization model is very convenient, and also serves to specify the parameters of other materials, and other models too.

GURSON-TVERGAARD-NEEDLEMAN (GTN) PARAMETERS OF DP STEELS WITH DIFFERENT ROLLING DIRECTIONS WERE DETERMINED AND INVESTIGATED AT DIFFERENT STRAIN RATES

SIMILARTY RATE: 6%

REFERENCES

[1] A. S. Podder, D. Bhattacharjee, and R. K. Ray, "Effect of martensite on the mechanical behavior of ferrite-bainite dual phase steels," *ISIJ Int.*, vol. 47, no. 7, pp. 1058–1064, 2007, doi: 10.2355/isijinternational.47.1058.

[2] C. M. Gómora, R. R. Ambriz, C. J. García, I. Ruíz-López, and D. Jaramillo, "Dissimilar Dual Phase-Low Carbon Steel Joints by the GMAW Process Subjected to Impact Load," *Metals (Basel).*, vol. 12, no. 3, pp. 1–18, 2022, doi: 10.3390/met12030404.

[3] C. Sébastien Y.P.Allain, Irina Pushkareva, JulienTeixeira, Mohamed Gouné, "Dual-Phase Steels: The First Family of Advanced High Strength Steels," *Encycl. Mater. Met. Alloy.*, 2022.

[4] S. Kang and H. Kwon: s, *No TitleMetall. Tran*. 1987.

[5] "www.arcelormittal.com." .

[6] M. Achouri, G. Germain, P. Dal Santo, and D. Saidane, "Experimental characterization and numerical modeling of micromechanical damage under different stress states," *Mater. Des.*, vol. 50, pp. 207–222, 2013, doi: 10.1016/j.matdes.2013.02.075.

[7] M. Feucht, D.-Z. Sun, T. Erhart, and T. Frank, "Recent development and applications of the Gurson model," in *LS-DYNA Anwenderforum*, 2006.

[8] F. Feng *et al.*, "Application of a GTN damage model predicting the fracture of 5052-O aluminum alloy high-speed electromagnetic impaction," *Metals (Basel).*, vol. 8, no. 10, 2018, doi: 10.3390/met8100761.

[9] K. L. Nielsen and V. Tvergaard, "Ductile shear failure or plug failure of spot welds modelled by modified Gurson model," *Eng. Fract. Mech.*, vol. 77, no. 7, pp. 1031–1047, 2010, doi: 10.1016/j.engfracmech.2010.02.031.

[10] R. O. Santos *et al.*, "Damage identification parameters of dual-phase 600-800 steels based on experimental void analysis and finite element simulations," *J. Mater. Res. Technol.*, vol. 8, no. 1, pp. 644–659, 2019, doi: 10.1016/j.jmrt.2018.04.017.

[11] M. H. Miloud, I. Zidane, and M. Mendas, "Coupled identification of the hardening behavior laws and Gurson–Tvergaard–Needleman damage parameters - validation on tear test of 12NiCr6 CT specimen," *Frat. ed Integrita Strutt.*, vol. 13, no. 49, pp. 630–642, 2019, doi: 10.3221/IGF-ESIS.49.57.

[12] F. Andrade and M. Feucht, "A comparison of damage and failure models for the failure prediction of dual-phase steels," 2017.

[13] C. Netrasiri and S. Suranuntchai, "Damage curve determination of dual phase steel based on gtn mode-l failure criteria," *Int. J. Mech. Eng. Robot. Res.*, 2016, doi: 10.18178/ijmerr.5.4.268-271.

[14] Y. Bao and T. Wierzbicki, "On fracture locus in the equivalent strain and stress triaxiality space," *Int. J. Mech. Sci.*, 2004, doi: 10.1016/j.ijmecsci.2004.02.006.

[15] H. Chalal and F. Abed-Meraim, "Determination of forming limit diagrams based on ductile damage models and necking criteria," *Lat. Am. J. Solids Struct.*, vol. 14, no. 10, pp. 1872–1892, 2017, doi: 10.1590/1679-78253481.

[16] M. Achouri, G. Germain, P. Dal Santo, and D. Saidane, "Numerical integration of an advanced Gurson model for shear loading: Application to the blanking process," *Comput. Mater. Sci.*, vol. 72, pp. 62–67, 2013, doi: 10.1016/j.commatsci.2013.01.035.

[17] N. STANDER, W. ROUX, T. GOEL, T. EGGLESTON, and K. E. N. CRAIG, *LS-OPT User ' s Manual: A DESIGN OPTIMIZATION AND PROBABILISTIC ANALYSIS TOOL*, no. February. 2012.

[18] N. A. Tvergaard, V, "Analysis of the cup-cone fracture in a round tensile bar," 1984.

[19] M. Springmann and M. Kuna, "Determination of ductile damage parameters by local deformation fields: Measurement and simulation," *Arch. Appl. Mech.*, vol. 75, no. 10–12, pp. 775–797, 2006, doi: 10.1007/s00419-006-0033-9.